Ferromagnetic nano-conductive filament formed in $Ni/TiO_2/Pt$ resistive-switching memory

Shintaro Otsuka, Yoshifumi Hamada, Tomohiro Shimizu & Shoso Shingubara

Applied Physics A
Materials Science & Processing

ISSN 0947-8396
Volume 118
Number 2

Appl. Phys. A (2015) 118:613-619
DOI 10.1007/s00339-014-8769-5

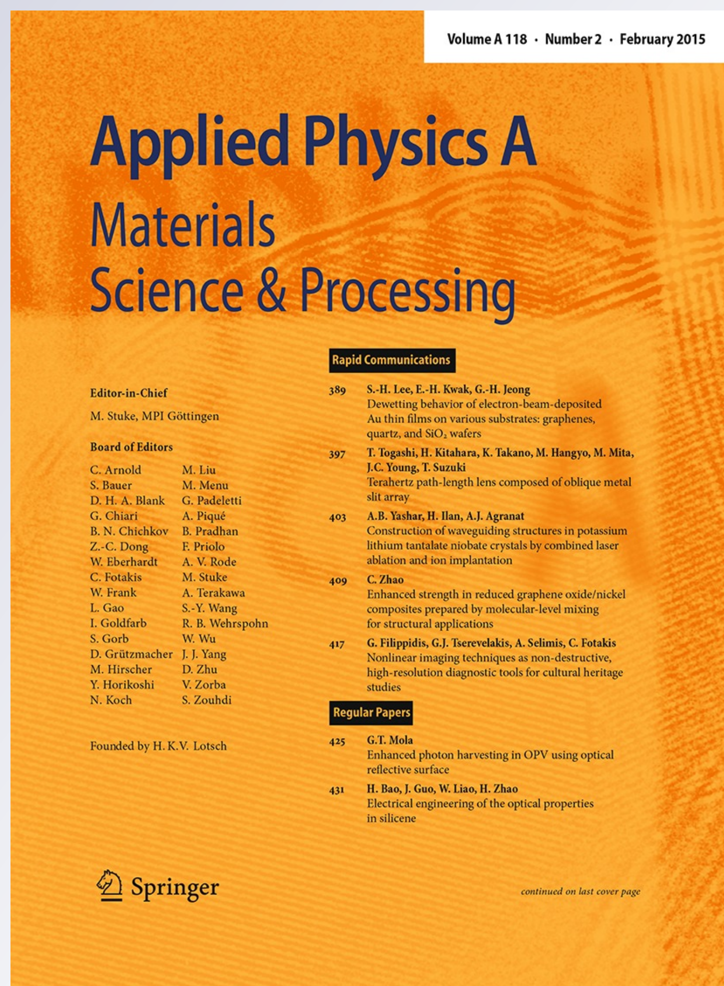

Springer

Your article is protected by copyright and all rights are held exclusively by Springer-Verlag Berlin Heidelberg. This e-offprint is for personal use only and shall not be self-archived in electronic repositories. If you wish to self-archive your article, please use the accepted manuscript version for posting on your own website. You may further deposit the accepted manuscript version in any repository, provided it is only made publicly available 12 months after official publication or later and provided acknowledgement is given to the original source of publication and a link is inserted to the published article on Springer's website. The link must be accompanied by the following text: "The final publication is available at link.springer.com".

Springer

Author's personal copy

Appl. Phys. A (2015) 118:613–619
DOI 10.1007/s00339-014-8769-5

Applied Physics A
Materials Science & Processing

Ferromagnetic nano-conductive filament formed in $Ni/TiO_2/Pt$ resistive-switching memory

Shintaro Otsuka · Yoshifumi Hamada · Tomohiro Shimizu · Shoso Shingubara

Received: 26 June 2014 / Accepted: 4 September 2014 / Published online: 17 September 2014
© Springer-Verlag Berlin Heidelberg 2014

Abstract There is a question whether the conductive filament (CF) formed in the oxide layer of a resistive-switching random access memory is made of oxygen vacancies or metallic atoms. We investigated the CF of $Ni/TiO_2/Pt$ device using temperature coefficient of resistance (TCR), anisotropic magnetoresistance (AMR), and cross-sectional transmission electron microscopy with energy dispersive X-ray analysis (TEM-EDX). The low resistance state (LRS) of the device showed metallic property by TCR measurement. Furthermore, the device in the LRS showed AMR, which was a direct evidence of the formation of ferromagnetic CF. The cross-sectional TEM-EDX observation revealed that a nano-sized Ni precipitation existed in the area nearby a conductive spot. It is intensively suggested that Ni atoms migrated from the adjacent Ni electrode to TiO_2 layer to form the nano-sized ferromagnetic CF.

1 Introduction

Resistive-switching (RS) random access memory is expected to become one of next generation non-volatile memories [1, 2], because of its scalability with respect to downsizing [3], potential for the reduction of power consumption [4], and high switching speed [5]. The structure of the RS memory device is simple, similar to that of a capacitor, consisting of two electrodes and an oxide thin film, such as a transition metal oxide or perovskite oxide, in between [6]. The proposed mechanisms can be classified into two models [7]. One is the filament model, which involves the formation and ruptures of a conductive filament (CF) formed in an oxide layer with soft breakdown. The device switches between a low resistance state (LRS) and a high resistance state (HRS) corresponding to connection and disconnection of the CF. There are two types of CFs: a metallic CF and an oxygen vacancy CF [8, 9]. In the filament model, resistive switching can be achieved with the same bias polarity and is thus called unipolar switching behavior. The other model is the interface model with a redox reaction at the interface between the electrode and the oxide layer. This model usually shows bipolar switching behavior [6].

Recently, it has been reported that CF in NiO-based RS memory had ferromagnetism [10, 11]. However, existence of ferromagnetism of individual CF of LRS has not been clarified yet, because superconducting quantum interference device was used to detect magnetization of CF. Only average property of a large number of CFs was measured in this case. If ferromagnetic CF exists, this suggests the possibility of both an RS memory and spintronics device. The aim of the present study was to confirm existence of a ferromagnetic CF by focusing on temperature coefficient of resistance (TCR), anisotropic magnetoresistance (AMR) [12, 13], and cross-sectional transmission electron microscopy with energy dispersive X-ray analysis (TEM-EDX). To this end, we prepared $Ni/TiO_2/Pt$ device that had ferromagnetic electrodes made of Ni and oxide layer made of the oxide of a non-ferromagnetic metal. The reason for using non-ferromagnetic metal oxide is to examine possibility of formation of ferromagnetic CF by the migration of ferromagnetic Ni metals into the oxide layer from the electrode.

S. Otsuka (✉) · Y. Hamada · T. Shimizu · S. Shingubara
Graduate School of Science and Technology, Kansai University, Suita, Osaka 564-8680, Japan
e-mail: k788955@kansai-u.ac.jp

S. Shingubara
e-mail: shingu@kansai-u.ac.jp

Author's personal copy

2 Experiment

The fabricated device has a simple crossbar structure formed on a thermally oxidized Si substrate, as shown in Fig. 1a. The device size is 6 × 6 μm^2. Figure 1b illustrates the cross section of the Ni/TiO_2/Pt structure. First, a Pt/Ti layer (30/5 nm) was deposited as a bottom electrode by direct current (DC) sputtering. Then, a TiO_2 (10 nm) layer was deposited on the Pt electrode by DC reactive sputtering using Ar and O_2 gases. Finally, a Ni layer (50 nm) was deposited by DC sputtering as a ferromagnetic top electrode. Chemical composition analysis of the TiO_2 film was performed by X-ray photoelectron spectroscopy (Shimazu ESCA-3400) using a magnesium anode (Mg Kα radiation of 1,253.6 eV). Au $4f_{7/2}$ (84.0 eV) was used as an internal standard for energy calibration. The atomic composition of the reactively sputtered oxide film was analyzed, the results of which revealed the films to be TiO_2. The electrical measurements of the device were taken at 300 K in air, where the current is limited to prevent the complete dielectric breakdown of the device. Figure 1c shows schematic of resistance network of the device and the electrodes. Resistance of the device in the LRS is smaller than that of the electrodes. To eliminate components of resistance of electrodes, a four-probe method was used when the TCR and AMR were measured. We could measure the resistance of the filament in the device by the method. In the HRS, a two-probe method was used during measurements because resistance of the HRS is much greater than that of electrodes. AMR was measured at 300 K. The morphology of the device was characterized by scanning electron microscope (SEM; JEOL JSM-7500F) and TEM-EDX (JEOL JEM-2100F).

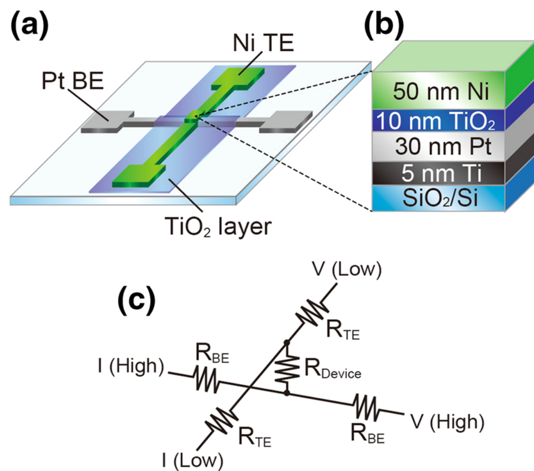

Fig. 1 Schematics of **a** the crossbar RS device structure and **b** the cross section of the device. **c** Shows the schematic of resistance network of the top electrode (R_{TE}), the bottom electrode (R_{BE}), and the device (R_{Device})

3 Results and discussion

The device was operated under unipolar operation mode, suggesting the unipolar switching mechanism. Figure 2a shows the typical unipolar RS characteristic. As the positive bias was applied to the Pt electrode, the current increased abruptly at 1.9 V. This indicated that an HRS-to-LRS transition occurred corresponding to the SET process. When the bias with the same polarity was applied again, the current decreased abruptly to a low value, which corresponded to the RESET process. The device switched reversibly between HRS and LRS under a DC voltage in the same voltage direction. The filament model accounts for the switching mechanism of the device. Figure 2b shows the endurance of RS behavior by sweeping DC voltage, where the read voltage is 0.1 V. At first, the device showed small current–voltage hysteresis loops. After several cycles, large hysteresis loops were observed. This RS corresponded to the forming process. After the forming process, RS phenomena with a high HRS/LRS ratio occurred.

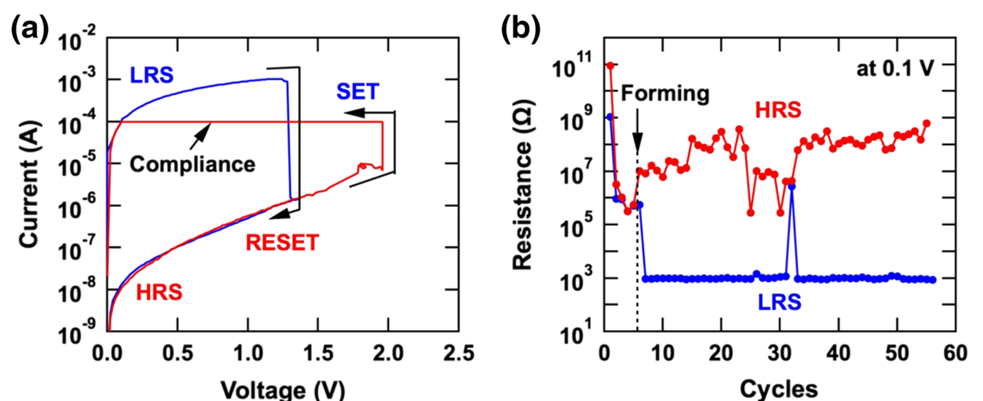

Fig. 2 **a** Typical unipolar RS characteristics. The current compliance value for the SET process is 0.1 mA. **b** Endurance characteristics under DC switching sweep mode. Readout voltage is 0.1 V

Author's personal copy

Figure 3 shows temperature dependence of the resistance for the LRS. The resistance of the LRS decreases almost linearly with temperature as the temperature is lowered from 300 to 50 K, indicating that the CF has a metallic conduction property. The inset shows the *I*–*V* characteristics of the LRS at 300 and 9.8 K. The linear *I*–*V* characteristics for both cases indicated that there is no Schottky barrier nor tunneling barrier in the LRS, and metallic conduction is suggested. The residual resistivity ratio (RRR), which can be expressed as RRR = $R_{300\ K}/R_{10\ K}$, is 1.45. This value is much smaller than that of the bulk pure Ni. It is suggested that the conductive electrons in the CF are scattered by lattice imperfections such as surfaces, grain boundaries, and impurities [14, 15]. In addition, TCR is calculated via TCR = $(1/R_0) \cdot (dR/dT)$ [15], where T is the temperature, R is the resistance, and R_0 is the resistance at 273 K. The TCR of the device from 273 to 293 K is 1.2×10^{-3}/K, which is much smaller than that of bulk pure Ni (6.1×10^{-3}/K) [16] but comparable to that of a 30-nm diameter Ni nano-wire (2×10^{-3}/K) [15]. Moreover, the TCR of our device is similar to that of a Ni/ZrO_2/Pt device (1.27–2.20×10^{-3}/K) [17]. This suggests that the metallic behavior of the LRS stems from a metallic Ni CF with a diameter of a few tens of nanometers. However, it is reported that TCR of oxygen vacancies CF in a Cu/Ta_2O_5/Pt device is 1.3×10^{-3}/K [18]. It is not easy to determine whether CF is made of metals or oxygen vacancies by the TCR only; therefore, we focused on magnetoresistance property of CF.

To examine magnetic characteristics of the device in the LRS, we measured magnetoresistance of the LRS as shown in Fig. 4, where the directions of the external magnetic field are shown in the schematics. The magnetic field H_x is

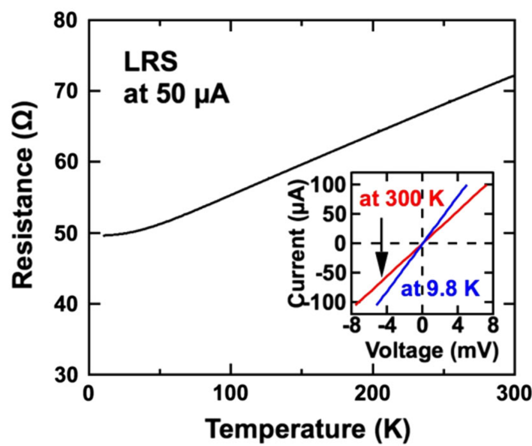

Fig. 3 Temperature dependence of resistance at a constant current of 50 µA. The inset shows *I*–*V* characteristics in the LRS at 300 and 9.8 K

in-plane to the substrate and perpendicular to the Ni top electrode. H_y is also in-plane and parallel to the Ni electrode. H_z is perpendicular to the substrate. MR ratio is defined as $\Delta R/R = \{R(H) - R(H_0)\}/R(H_0) \times 100$ (%) [19], where $R(H)$ is the resistance under the external magnetic field and $R(H_0)$ is the resistance at zero field. It should be noted that AMR was observed in the LRS. The AMR showed a convexity under the applied fields H_x and H_y. A concave AMR was observed under the field H_z. As a reference, AMR of a Ni wire with 6 um width and 50 nm thickness is shown in Fig. 5, where the configuration of the Ni wire and the directions of the current and external magnetic field are illustrated too. The inset figures are enlarged views of the regions marked with rectangle. We will discuss how the shape of the AMR curve depends on the direction of the current flowing into the Ni wire and the device. AMR, which occurred in ferromagnetic transition metals, depends on the direction of the magnetization with respect to the electric current direction in the material [12, 13]. The theoretical basis takes into account spin orbit coupling and *d* band splitting. AMR is given by

$$\rho(\theta) = \rho_\perp \sin^2\theta + \rho_{//} \cos^2\theta$$

where θ is angle between the current in material and the direction of the magnetization and the $\rho_{//}$ and $\rho_\perp$ are electrical resistivities parallel and perpendicular to direction of magnetization, respectively. In the case of ferromagnetic transition metals and alloys, $\rho_{//}$ is generally greater than $\rho_\perp$. The parallel and perpendicular configurations show AMR with concave and convex shapes, respectively. These shapes are caused by the orientation effect that depends on the direction of the spontaneous magnetization and the change of magnetic domain caused by domain wall movement. In the Ni wire, the current flows along the *y*-axis, the AMR exhibits concavity, because the current is parallel to the magnetic field, as shown in Fig. 5b. In the device, concave AMR is observed when the magnetic field is applied along the *z*-axis, as shown in Fig. 4c. This is because the current flowing into the device is perpendicular to the substrate and parallel to the field. From above results, we infer that the observed AMR in the device is originated from the ferromagnetic CF formed in the TiO_2 layer. The relationship between the currents I_{CF} in the ferromagnetic CF and external magnetic fields is illustrated in Fig. 4. Coercivities (H_c) of the device are about 50 mT for H_x, about 70 mT for H_y, and about 100 mT for H_z, which are much larger than those of the Ni wire (H_x: 1 mT, H_y: 1 mT, H_z: 70 mT), as shown in Fig. 5, where coercivities are determined by the switching field of AMR. Coercivity values of the Ni wire were comparable to those reported for Ni film and lines [20]. In the device, hysteresis loops are clearly observed under field H_z because

Author's personal copy

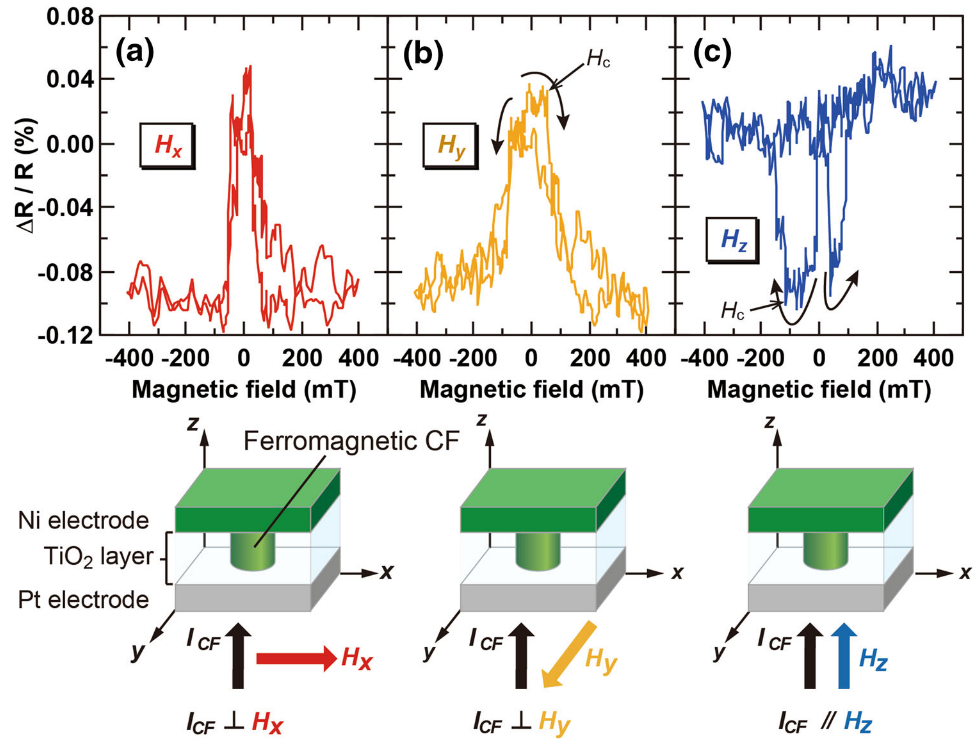

Fig. 4 Magnetoresistance characteristics in the LRS. Directions of the external magnetic field are **a** H_x, **b** H_y, and **c** H_z. *Arrows* in the figures indicate direction of the hysteresis loop. The lower drawings illustrate the geometry between the current I_{CF} into the CF and the external magnetic field H during the magnetoresistance measurement

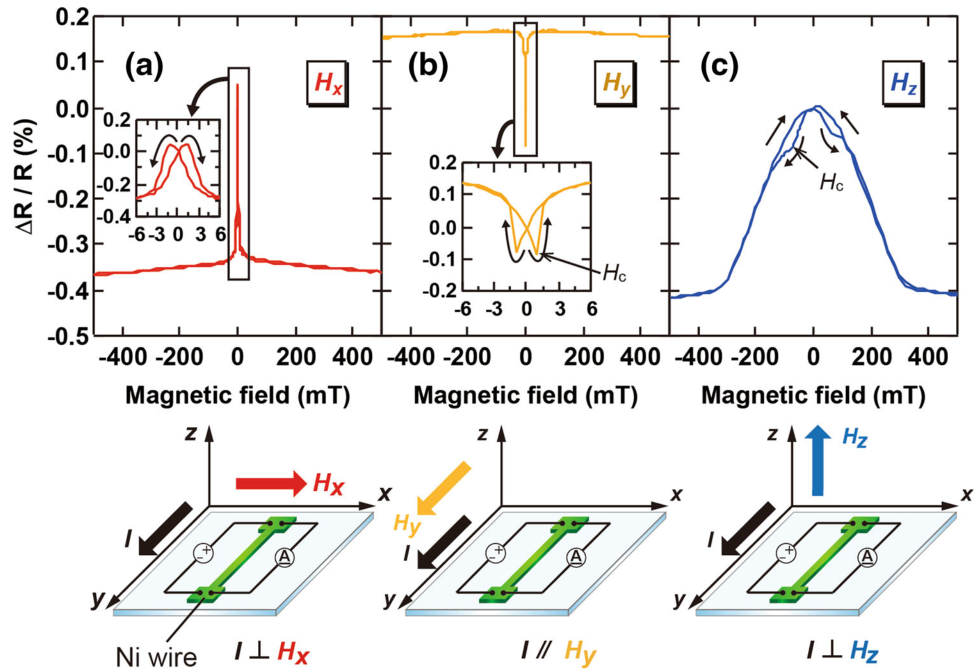

Fig. 5 AMR characteristics of the Ni wire. Directions of the external magnetic field are **a** H_x, **b** H_y, and **c** H_z. *Arrows* in the figures indicate direction of the hysteresis loop. The *inset* plots are enlarged views of the regions marked with *rectangle*. (The units of the *inset* axes are the same as in the main figure.) The lower images illustrate the geometry between the directions of the current in the Ni wire and the external magnetic field during the magnetoresistance measurement

of the large coercivity. Coercivities of the device are increased by the nano-sized effect derived from the shape magnetic anisotropy [20–22]. Therefore, diameter of the ferromagnetic CF in the device is supposed to be nano-scale. The maximum AMR ratio of the Ni lines is 0.75 % [20]. The observed AMR in our device is approximately 0.1 %, which is smaller than that of the Ni film. It is suggested that the ferromagnetic Ni CF included lattice imperfections that is expected from the temperature dependence of resistance.

Author's personal copy

We attempted to identify the location where the ferromagnetic CF was formed. Figure 6 shows the top-view SEM image of the device in the LRS after the forming process. The vertical bar is the top electrode, and the horizontal bar is the bottom electrode. Before the forming process, the surface of the top electrode showed no irregular feature (data not shown); however, after the forming process, it featured bright spots as shown in Fig. 6. An inset shows an enlarged view of these bright spots. Three protrusions with diameters of about 280, 90, and 50 nm were observed. The deformation of the top electrode is supposed to be caused by an explosion due to Joule heating during the forming process [9, 23]. We confirmed that devices having several protrusion spots similar to Fig. 6 still exhibit stable switching phenomena. Therefore, we believe that the protrusions are related to conductive spots where the ferromagnetic CF is formed.

To observe the ferromagnetic CF, cross-sectional TEM-EDX analysis was carried out for largest and second largest of conductive spots. The largest spot has a dome-like shape due to the explosion that occurred during the forming process (data not shown). This spot no longer contributes to the electrical conduction because the top electrode does not contact the TiO_2 layer. The TEM bright-field image of the cross section of as-deposited sample and the second largest spot are shown in Fig. 7a, b, respectively. The explosion changes the features of the TiO_2 layer under the protrusion. The bright areas in the TiO_2 layer are voids that were presumably formed as a result of Joule heating which generates O_2 molecules in the TiO_2 layer [24]. We used TEM-EDX to analyze the composition of the as-deposited sample and the sample after the formation at the location under second largest spot. Figure 7c, d shows the distribution of the atomic ratio of Ni, Ti, and Pt for each position along the dashed lines in TEM images. In the line (c), the amounts of Ni and Pt decrease toward the TiO_2 layer and each layer is clearly distinctive. By contrast, in the line (d), the distributions of Ni and Pt exhibit shoulders around 23–28 nm corresponding to the TiO_2 layer. This suggests that the area contains Ni and Pt atoms. Joule heating causes the diffusion of Ni electrode into the TiO_2 layer. We expect that ferromagnetic CF, which consists of precipitated Ni atoms, exists around protrusions. However, accurate location of the ferromagnetic CF is unclear because the smallest protrusion is not observed, and a prepared TEM specimen is fragmentary. To understand the formation of the ferromagnetic CF more in detail, in situ dynamical observation using TEM-EDX would be necessary.

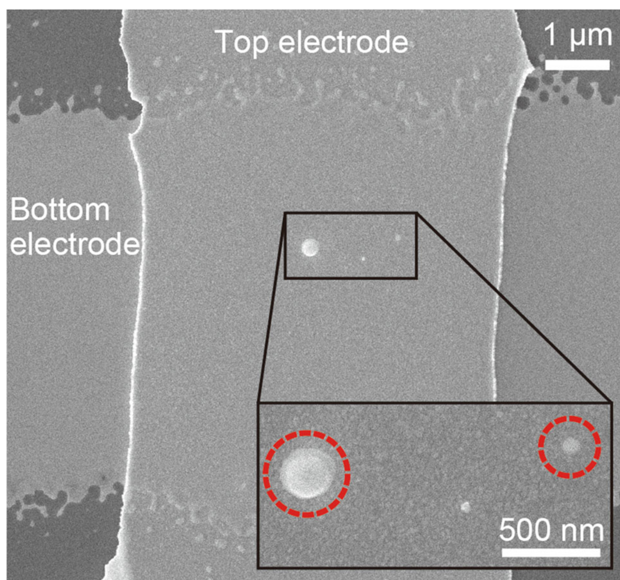

Fig. 6 SEM image of the *top* view of the crossbar RS device in the LRS after the forming process. *Inset* is an enlarged view of the protrusions. *Circles* indicate the observed protrusions using the cross-sectional TEM

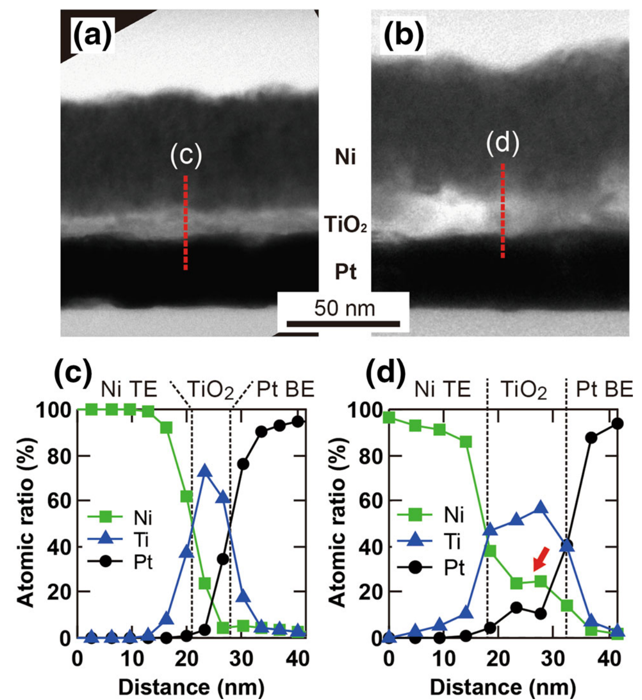

Fig. 7 Bright-field TEM images of the cross section of **a** as-deposited sample and **b** the second largest spot. **c** and **d** show distributions of the atomic ratio of Ni, Ti, and Pt as determined by EDX for each position along the dashed lines in TEM images. The *arrow* in figure **d** indicates the position of the shoulder for the Ni atomic ratio

We cannot distinguish a metallic CF and an oxygen vacancy CF by TCR measurement only; however, the observed AMR is a clear evidence of ferromagnetic CF. Because RS phenomenon occurs in the same voltage direction, the ferromagnetic CF may be formed due to thermal diffusion assisted by a Joule heating effect of Ni atoms from the adjacent Ni electrode to TiO_2 layer, rather than ion migration of Ni ions. In the TiO_2-based

Author's personal copy

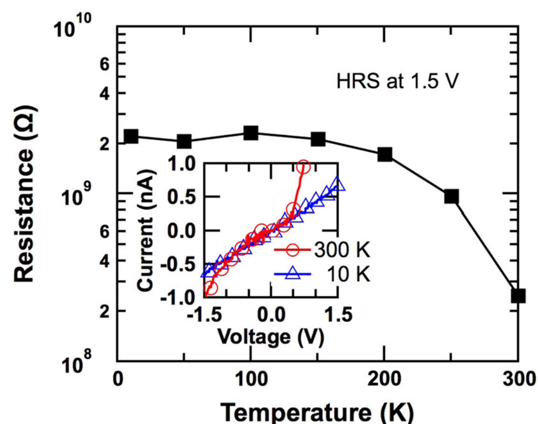

Fig. 8 Temperature dependence of resistance of the HRS at 1.5 V. The inset shows *I–V* characteristics at 300 and 10 K

device, unipolar as well as bipolar RS phenomena have been explained by oxygen vacancy CF [9, 24–27]. On the other hand, in the case of unipolar device, it is well known that CF is attributed to Magnéli structure [9]. Therefore, the Magnéli structure might be formed in our device. However, we could not find the structure because TiO_2 layer was too thin. It seemed that Joule heating occurred by a large current that flew through the Magnéli structure; then, Ni atoms were diffused away. Generally, Pt was used as the both electrodes for TiO_x-based RS memory, and the thickness of the TiO_x layer was thick enough (20–57 nm [9, 24–27]) compared with that of our device, so that electrode material might not diffused in the TiO_x layer.

In the HRS, the resistance at 1.5 V increases with decreasing temperature in the temperature range from 300 to 200 K and remains almost constant at temperature lower than 200 K, as shown in Fig. 8. *I–V* characteristics at 300 and 10 K are shown in the inset. The *I–V* characteristic shows nonlinearity at 300 K. The tunneling current passing through the insulating layer, which was independent of temperature, is dominant at a low temperature [14]. AMR was not observed for either of three directions in the HRS (data not shown). It is suggested that the ferromagnetic CF was ruptured during the RESET process, probably due to dissolution and/or oxidation of Ni atoms in the ferromagnetic CF. Joule heating by large current may be one of reasons for the RESET process.

The device with ferromagnetic CF exhibited both RS memory and spintronics device properties. Although the observed magnitude of AMR is small, there is the possibility of obtaining a large MR [28]. We expect that the ferromagnetic CF will pave the way to a new multi-functional device with both spin-dependent and electrical field-dependent conduction properties, not only for memory but also for logic device functions as well.

4 Conclusion

We investigated existence of the ferromagnetic CF in Ni/TiO_2/Pt device with unipolar RS characteristic. The temperature dependence of the resistance of the CF formed in the device exhibited metallic conduction properties. It was shown that AMR occurred in the LRS, which strongly suggested that a ferromagnetic CF was formed in the TiO_2 layer. Precipitated Ni was observed in the TiO_2 layer under the protrusion using cross-sectional TEM-EDX. From the above results, it is suggested that Ni atoms were diffused from the adjacent Ni electrode to form the ferromagnetic CF.

Acknowledgments This work is supported by a Research Fellowship from the Japan Society for the Promotion of Science (JSPS). This work is partially supported by the Strategic Project to Support the Formation of Research Bases at Private Universities: the Matching Fund Subsidy from Ministry of Education, Culture, Sports, Science, and Technology (MEXT).

References

1. R. Waser, R. Dittmann, G. Staikov, K. Szot, Adv. Mater. **21**, 2632 (2009)
2. H. Akinaga, Jpn. J. Appl. Phys. **52**, 100001 (2013)
3. I. G. Baek, M. S. Lee, S. Seo, M.-J. Lee, D. H. Seo, D.-S. Suh, J. C. Park, S. O. Park, T. I. Kim, I. K. Yoo, U.-I. Chung, and J. T. Moon, IEDM Tech. Dig., 587 (2004)
4. K. Tsunoda, K. Kinoshita, H. Noshiro, Y. Yamazaki, T. Iizuka, Y. Ito, A. Takahashi, A. Okano, Y. Sato, T. Fukano, M. Aoki, and Y. Sugiyama,IEDM Tech. Dig., 767 (2007)
5. Y. Hosoi, Y. Tamai, T. Ohnishi, K. Ishihara, T. Shibuya, Y. Inoue, S. Yamazaki, T. Nakano, S. Ohnishi, N. Awaya, H. Inoue, H. Shima, H. Akinaga, H. Takagi, H. Akoh, and Y. Tokura, IEDM Tech. Dig., 793 (2006)
6. A. Sawa, Mater. Today **11**, 28 (2008)
7. H. Akinaga, H. Shima, Proc. IEEE **98**, 2237 (2010)
8. X. Wu, D. Cha, M. Bosman, N. Raghavan, D.B. Migas, V.E. Borisenko, X.-X. Zhang, K. Li, K.-L. Pey, J. Appl. Phys. **113**, 114503 (2013)
9. D.-H. Kwon, M.K. Kim, H.J. Jang, M.J. Jeon, H.M. Lee, H.G. Kim, X.-S. Li, G.-S. Park, B. Lee, S. Han, M. Kim, S.C. Hwang, Nat. Nanotechnol. **5**, 148 (2010)
10. J.Y. Son, C.H. Kim, J.H. Cho, Y.H. Shin, H.M. Jang, ACS Nano **4**, 3288 (2010)
11. X.L. Wang, P.S. Ku, Q. Shao, W.F. Cheng, C.W. Leung, A. Ruotolo, Appl. Phys. Lett. **103**, 223508 (2013)
12. T.R. McGuire, R.I. Potter, IEEE Trans Magn **11**, 1018 (1975)
13. J. Smit, Physica **17**(6), 612–617 (1951)
14. K. Okamoto, M. Tada, T. Sakamoto, M. Miyamura, N. Banno, N. Iguchi, and H. Hada, IEDM Tech. Dig., 12.2.1. (2011)
15. Y. Rheem, Y.B. Yoo, P.W. Beyermann, V.N. Myung, Nanotechnology **18**, 015202 (2007)
16. American institute of physics handbook, United States of America, 1972, pp 9–39
17. J. Sun, Q. Liu, H. Xie, X. Wu, F. Xu, T. Xu, S. Long, H. Lv, Y. Li, L. Sun, M. Liu, Appl. Phys. Lett. **102**, 053502 (2013)
18. T. Liu, M. Verma, Y. Kang, M.K. Orlowski, ECS Solid State Lett. **1**, Q11 (2012)

Author's personal copy

19. Y. Rheem, B.Y. Yoo, W.P. Beyermann, N.V. Myung, Phys. Status Solidi **204**, 4004 (2007)
20. J.I. Martin, M. Velez, J.M. Alameda, F. Briones, J.L. Vicent, J. Magn. Mater. **240**, 14 (2002)
21. T. Shimizu, N. Nagayanagi, Y. Fujii, O. Yaegashi, G.R. Wu, H. Sakaue, T. Takahagi, S. Sakata, H. Kusaka, S. Shingubara, Trans. Magn. Soc. Jpn. **4**, 231 (2004)
22. S. Shingubara, K. Morimoto, M. Nagayanagi, T. Shimizu, O. Yaegashi, G.R. Wu, H. Sakaue, T. Takahagi, K. Takase, J. Magn. Magn. Mater. **272**, 1598 (2004)
23. H. Kondo, M. Arita, T. Fujii, H. Kaji, M. Moniwa, T. Yamaguchi, I. Fujiwara, M. Yoshimaru, Y. Takahashi, Jpn. J. Appl. Phys. **50**, 081101 (2011)
24. J.J. Yang, F. Miao, M.D. Pickett, D.A.A. Ohlberg, C.N. Lau, R.S. Williams, Nanotechnology **20**, 215201 (2009)
25. J.J. Yang, M.D. Pickett, X. Li, D.A.A. Ohlberg, D.R. Stewart, R.S. Williams, Nat. Nanotechnol. **3**, 429 (2008)
26. Y.C. Bae, A.R. Lee, J.S. Kwak, H. Im, Y.H. Do, J.P. Hong, Appl. Phys. A **102**, 1009 (2011)
27. B.J. Choi, D.S. Jeong, S.K. Kim, C. Rohde, S. Choi, J.H. Oh, H.J. Kim, C.S. Hwang, K. Szot, R. Waser, B. Reichenberg, S. Tiedke, J. Appl. Phys. **98**, 033715 (2005)
28. K. Yakushiji, F. Ernult, H. Imamura, K. Yamane, S. Mitani, K. Takanashi, S. Takahashi, S. Maekawa, H. Fujimori, Nat. Mater. **4**, 57 (2005)